UMYU Scientifica, Vol. 5 NO. 1, March 2026, Pp 402 – 413
https://doi.org/10.56919/usci.2651.034
ISSN: 2955 – 1145 (print); 2955 – 1153 (online)
A periodical of the Faculty of Natural and Applied Sciences, UMYU, Katsina

ORIGINAL RESEARCH ARTICLE

Experimental Investigation of Thermal Behavior and Optical Performance of High-Power White LEDs under Variable Operating Conditions

Abdurrasheed B Magaji*[1], Shariff M Abdulkadir[2]
[1]Department of Physics, Faculty of Natural and Applied Sciences, Umaru Musa Yar'adua University, Katsina, Katsina State, Nigeria
[2]Department of Physics, Federal College of Education, Katsina, Katsina State, Nigeria

ABSTRACT
The performance and long-term reliability of high-power light-emitting diodes (LEDs) are strongly governed by junction temperature, which directly influences luminous output, efficiency, and device lifetime. While junction temperature is the fundamental parameter of interest, this study experimentally investigates the coupled thermal and optical behavior of high-power white LEDs by analyzing case temperature measurements, which serve as practical proxies for thermal performance. Three analyses were conducted: (i) luminous intensity variation with temperature for Luxeon Star LEDs driven at 100 mA, 200 mA, and 300 mA; (ii) transient thermal behavior of a 12 V DC LED module measured using both K-type thermocouple and infrared thermography; and (iii) thermal response of a 230 V AC LED lamp with integrated heat sink during 120 minutes of continuous operation. This study provides a novel multi-faceted comparative analysis by quantifying the measurement discrepancy between contact and non-contact thermometry under dynamic conditions, experimentally validating a first-order thermal model for a commercial AC LED lamp, and demonstrating current-dependent thermal resistance. Results demonstrate a clear inverse linear relationship between temperature and luminous output, with light output decreasing by approximately 4.5% over a 6°C rise at 300 mA drive current (temperature coefficient β = -0.62%/°C). Higher drive currents produce greater thermal stress and accelerated light degradation. Infrared measurements consistently reported temperatures 2–4°C higher than thermocouple readings due to emissivity and spatial averaging effects. The 230 V system exhibited stable thermal regulation, reaching steady-state after approximately 90 minutes with a thermal time constant τ = 22.3 ± 1.2 minutes (R^2 = 0.987), consistent with a first-order heat transfer model. The findings confirm that effective thermal management is essential for minimizing efficiency droop, preventing thermal runaway, and ensuring long-term reliability in high-power LED applications, including general illumination and visible light communication systems.

ARTICLE HISTORY
Received November 13, 2025
Accepted March 20, 2026
Published March 28 2026

KEYWORDS
High-power LED; thermal management; luminous degradation; infrared thermography; thermal time constant; efficiency droop

© The Author(s). This is an Open Access article distributed under the terms of the Creative Commons Attribution 4.0 License creativecommons.org

INTRODUCTION
Light-emitting diodes (LEDs) have revolutionized the lighting industry, emerging as the dominant solid-state lighting technology due to their superior efficiency, extended operational lifetime, compact form factor, and reduced environmental impact compared to conventional lighting systems like incandescent and fluorescent lamps (Schubert, 2006; Zukauskas et al., 2002). Their application has rapidly expanded beyond general illumination to encompass specialized fields such as automotive lighting, display backlighting, and emerging data communication technologies like visible light communication (VLC) (Komine & Nakagawa, 2004; Chi et al., 2015).

Despite these significant advantages, the performance and reliability of high-power LEDs are critically dependent on thermal management. The junction temperature, the temperature of the semiconductor p-n junction is a key parameter that governs luminous flux, spectral stability, electrical efficiency, and device reliability (Narendran & Gu, 2005; Meneghini et al., 2010). While direct measurement of junction temperature requires specialized techniques (such as forward voltage method), case temperature measurements provide practical and accessible proxies for assessing thermal performance, as they correlate with junction temperature through the device's thermal resistance.

The input electrical power (P_{elect}) is converted partly into light (P_{opt}) and partly into heat (P_{heat}). The heat generation rate is given by:

$$P_{heat} = P_{elect} - P_{opt} = I_F \times V_F - P_{opt} \quad (1)$$

Correspondence: Abdurrasheed B Magaji. Department of Physics, Faculty of Natural and Applied Sciences, Umaru Musa Yar'adua University, Katsina, Katsina State, Nigeria. ✉ abdulrasheed.magaji@umyu.edu.ng.
How to cite: Magaji, A. B., & Abdulkadir, S. M. (2026). Experimental Investigation of Thermal Behavior and Optical Performance of High-Power White LEDs under Variable Operating Conditions. *UMYU Scientifica*, 5(1), 402 – 413. https://doi.org/10.56919/usci.2651.034

where I_F is the forward current and V_F is the forward voltage. Operating LEDs at high drive currents to achieve greater light output inevitably leads to significant heat generation within the chip. This self-heating effect can trigger several degradation mechanisms, including enhanced non-radiative recombination, reduced internal quantum efficiency, phosphor thermal quenching in white LEDs, and accelerated aging of packaging materials, all of which culminate in reduced light output, color shifts, and a shortened operational lifespan (Gu et al., 2006; Tsao, 2014).

The detrimental effects of temperature on LED performance have been extensively documented. Foundational work by Schubert (2006) established that the efficiency of an LED decreases with increasing temperature primarily due to a reduction in internal quantum efficiency, as elevated temperatures increase the probability of non-radiative recombination via phonon emission. The light output power (Plight) as a function of temperature is often modeled with a negative linear coefficient:

$$P_{light}\,(T) = P_{light}\,(T_o)[1 + \beta(T_j - T_o)] \quad (2)$$

where β is the negative temperature coefficient of light output, typically ranging from -0.2% to -1.0% per °C for AlGaInP and InGaN-based LEDs. Narendran and Gu (2005) empirically demonstrated this linear decrease in luminous flux with rising junction temperature, a finding that underscores the need for accurate thermal prediction in system design.

The origin of this heat is primarily the self-heating effect resulting from high drive currents. Gu et al. (2006) reported that while increasing current yields higher light output, it also exponentially increases heat generation. If this heat is not effectively dissipated, it can lead to a positive feedback loop of thermal runaway, where increased temperature reduces efficiency, which in turn generates more heat for a given light output. This phenomenon is particularly critical in high-power applications (Meneghini et al., 2010; Zhang et al., 2016). The importance of the entire thermal path, from the junction through the package and heat sink to the ambient, was emphasized by Poppe and Lasance (2010), who advocated for standardized methods of thermal characterization. The total thermal resistance (R_{th}) from junction to ambient is defined as:

$$R_{thJA} = \frac{T_j - T_a}{P_{heat}} \quad (3)$$

where T_a is the ambient temperature. This parameter is crucial for predicting operating temperatures. Using this relationship, junction temperature can be estimated from measured case temperature if the thermal resistance between the junction and case (R_{thJA}) is known from manufacturer datasheets.

To study these effects, accurate temperature measurement is vital. Infrared (IR) thermography provides a non-contact method for obtaining a full two-dimensional temperature map of an LED's surface, which is invaluable for identifying hot spots and assessing temperature distribution (Kim et al., 2012; Shen et al., 2012). However, as noted by Farkas et al. (2013), IR measurements require careful correction for the surface's emissivity (ε) using the Stefan-Boltzmann law, $E = \varepsilon\sigma T^4$, to ensure accuracy. Conversely, thermocouples offer a simple and direct point measurement but may underestimate peak temperatures and are affected by the thermal contact resistance between the junction and the measurement point (Luo et al., 2017).

The primary tool for passive thermal regulation is the heat sink. Arik et al. (2007) demonstrated through modeling and experimentation that a properly designed heat sink can reduce junction temperature by up to 30%, dramatically slowing thermally activated aging processes. The transient thermal behavior of an LED mounted on a heat sink can be approximated by a first-order model:

$$T(t) = T_F - (T_F - T_i)e^{-t/\tau} \quad (4)$$

where T_i is the initial temperature, TF is the final steady-state temperature, and τ is the thermal time constant of the system. Studies on long-term reliability, such as those formalized in the IES LM-80 standard, confirm that maintaining lower operating temperatures is directly correlated with better lumen maintenance and longer useful life (Illuminating Engineering Society [IES], 2008).

Despite extensive documentation of LED thermal degradation mechanisms, few studies have provided integrated experimental validation across multiple device formats (discrete power LED, DC module, AC lamp) using simultaneous contact and non-contact thermometry under dynamically controlled conditions. Furthermore, quantitative validation of first-order thermal models for commercial lamps with integrated heat sinks, including extraction of thermal time constants and systematic comparison of measurement techniques, remains underexplored in the literature. The present study addresses this gap by providing a comprehensive experimental investigation that: (i) quantifies the relationship between drive current, temperature rise, and luminous degradation; (ii) compares contact and non-contact temperature measurement techniques under identical operating conditions; and (iii) experimentally validates first-order thermal modeling for a commercial AC LED lamp, extracting key thermal parameters for design optimization.

MATERIALS AND METHODS

2.1 Experimental Devices

Three types of high-power white LED devices were investigated in this study:

1. **Luxeon Star LED (LXHL-PW09, Lumileds):** A 1W high-power white LED with typical luminous flux of 45 lm at 350 mA. The device was mounted on a temperature-controlled aluminum platform with thermal interface material to ensure consistent thermal contact.
2. **12 V DC LED Module (SMD 5050, 3×1W):** A commercial module containing three 1W white LED chips

mounted on an aluminum substrate PCB. The module operates at 12V DC with typical current consumption of 300 mA.

3. **230 V AC LED Lamp (9W, Philips):** A commercial retrofit LED lamp with integrated aluminum heat sink and built-in constant current driver. The lamp contains multiple LED chips with phosphor conversion for white light generation. Complete specifications for all devices are summarized in Table 1.

2.2 Measurement Instruments

The following instruments were used for data acquisition. Temperature measurements were obtained using a digital thermocouple thermometer (Fluke 51-II) equipped with a K-type bead probe, offering an accuracy of ±0.5°C and a resolution of 0.1°C. To ensure consistent thermal contact, the probe was attached to the LED case surfaces using thermally conductive epoxy.

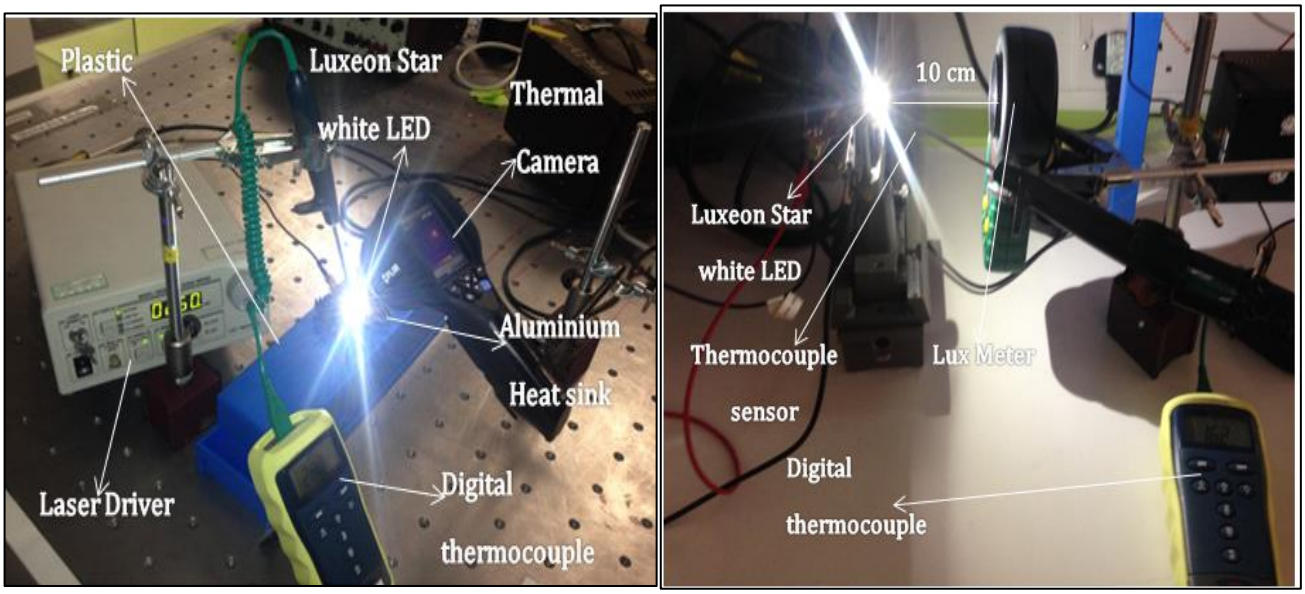

Figure 1: Experimental setup showing LED mounting configuration, thermocouple attachment, IR camera positioning, and lux meter geometry.

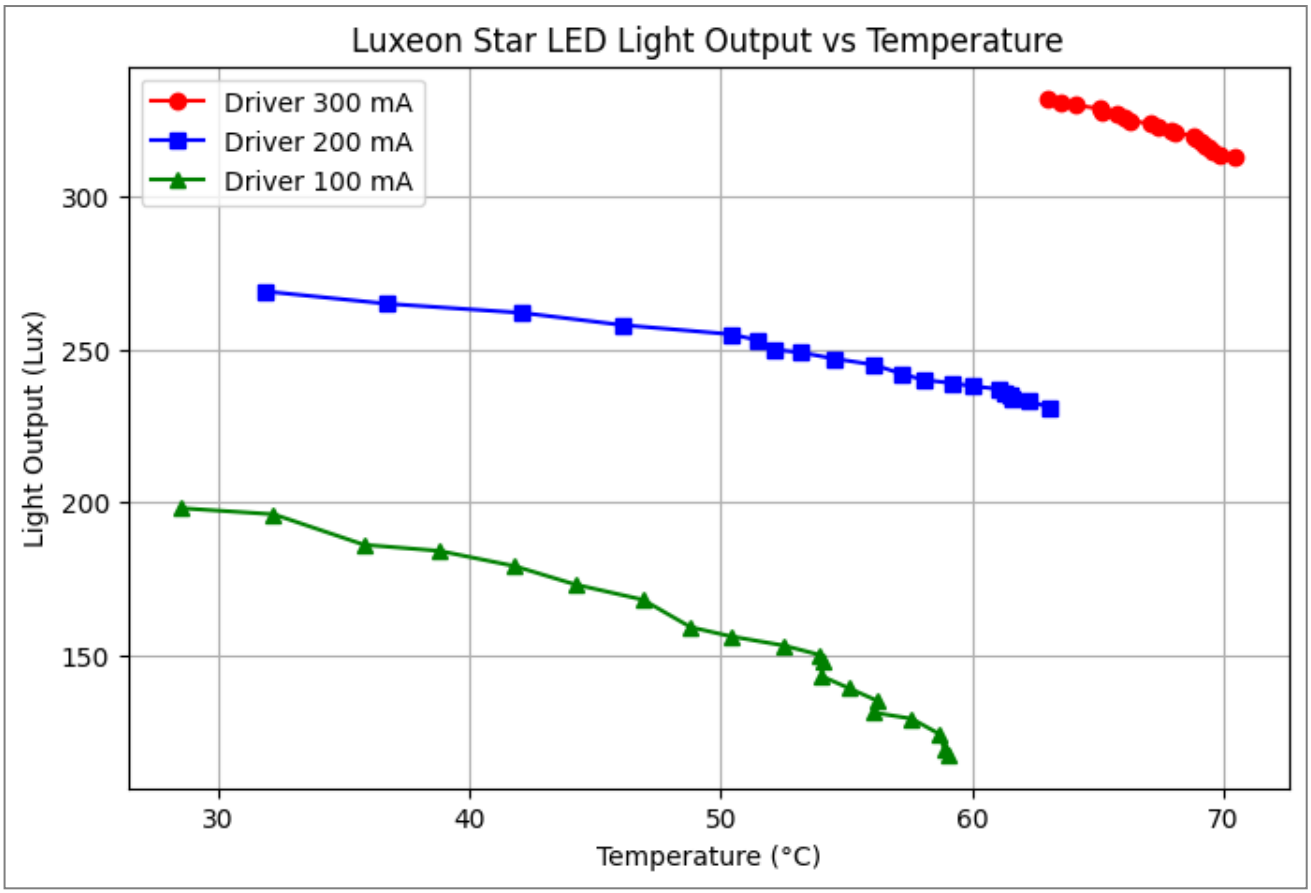

Figure 2: Relative luminous output versus case temperature for Luxeon Star LED at drive currents of 100 mA, 200 mA, and 300 mA. Error bars represent ±1 standard deviation from triplicate measurements.

Table 1: Specifications of LED Devices under Test

Device	Model	Power Rating	Forward Current	Luminous Flux	Thermal Resistance (R_{thJA})
Luxeon Star	LXHL-PW09	1W	350 mA (max)	45 lm @ 350 mA	15°C/W
12V DC Module	SMD 5050	3W	300 mA (total)	180 lm	12°C/W (per chip)
230V AC Lamp	9W Philips	9W	80 mA (typical)	800 lm	8°C/W (module)

Table 2: Temperature Coefficient of Luminous Output at Different Drive Currents

Drive Current (mA)	Temperature Range (°C)	β (%/°C)	R^2	95% Confidence Interval
100	35 - 55	-0.38 ± 0.04	0.962	(-0.42, -0.34)
200	48 - 68	-0.51 ± 0.05	0.971	(-0.56, -0.46)
300	64 - 70	-0.62 ± 0.06	0.954	(-0.68, -0.56)

Table 3: Comparison of Thermocouple and IR Temperature Measurements

Time (min)	Thermocouple Temp (°C)	IR Temp (°C)	Difference (°C)
0	25.0 ± 0.5	25.0 ± 1.0	0.0
10	42.3 ± 0.6	45.1 ± 1.1	2.8
20	51.8 ± 0.7	55.0 ± 1.2	3.2
30	55.2 ± 0.7	58.6 ± 1.2	3.4
40	56.8 ± 0.8	60.2 ± 1.3	3.4
50	57.5 ± 0.8	60.9 ± 1.3	3.4
60	57.9 ± 0.8	61.4 ± 1.3	3.5

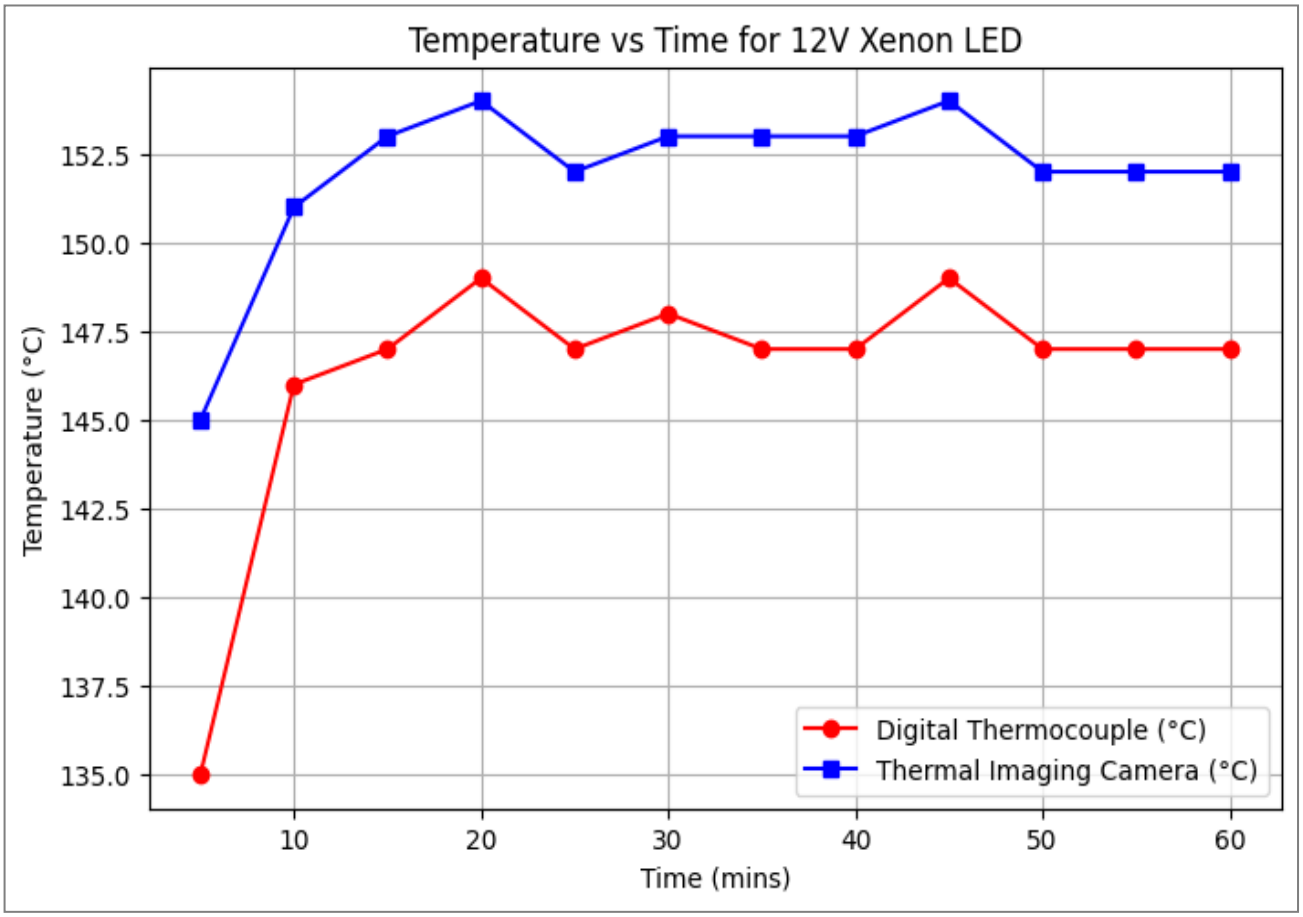

Figure 3: Temperature versus time for 12V LED module measured by K-type thermocouple and infrared thermography. Error bars represent ±1 standard deviation.

Thermal imaging was carried out using an infrared thermal imaging camera (FLIR E60), which has a resolution of 320 × 240 pixels, thermal sensitivity of less than 0.05°C, and an accuracy of ±1°C. The camera was calibrated at an emissivity value of ε = 0.95, which was determined through comparison with thermocouple measurements taken on black-painted reference surfaces.

Illuminance measurements were performed using a digital lux meter (TES-1335) with a measurement range of 0 to 400,000 lux and an accuracy of ±3%. The sensor was positioned at a fixed distance of 30 cm from the LED devices and oriented at a 45° angle to minimize direct glare and maintain consistent measurement geometry.

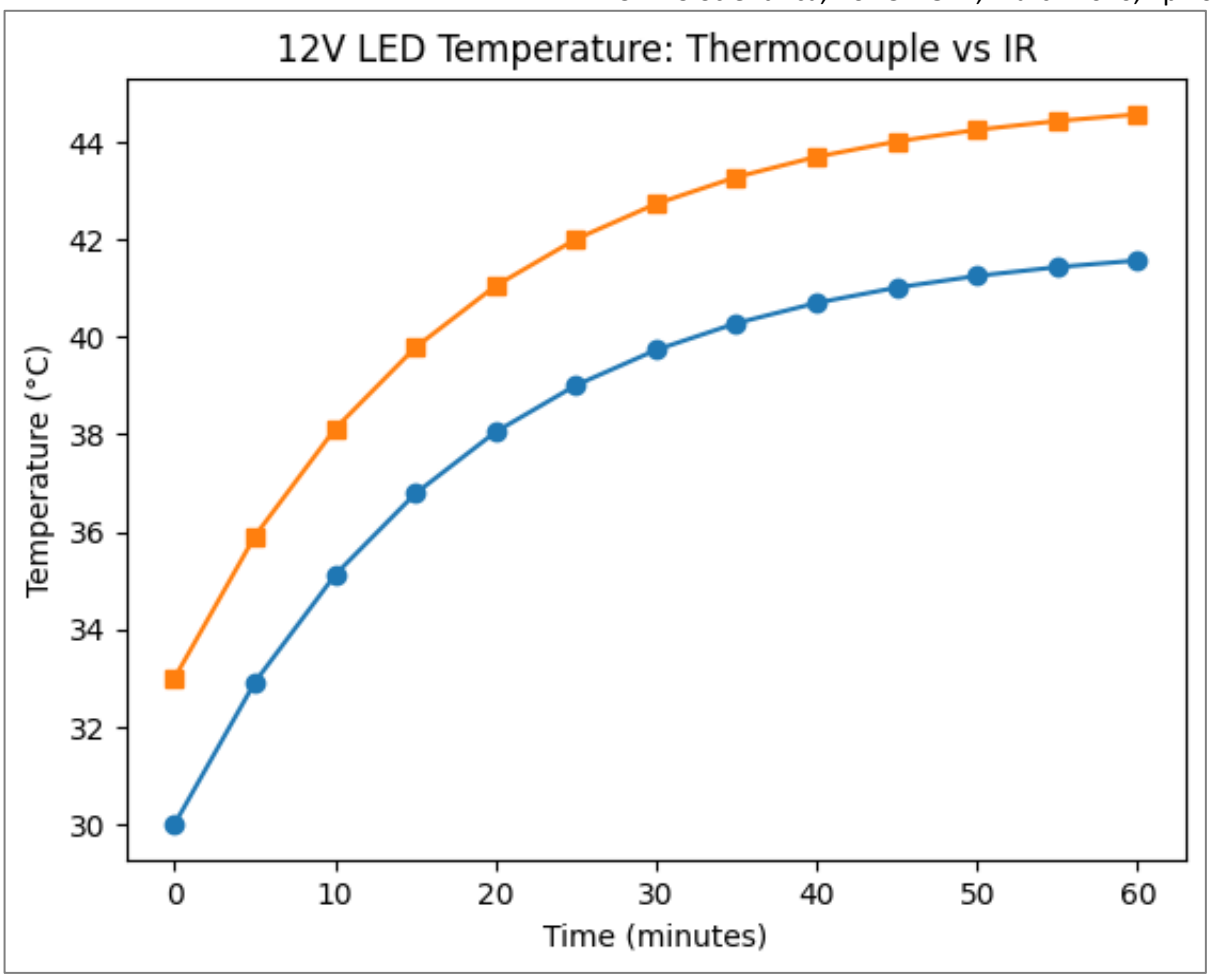

Figure 4: Direct comparison of thermocouple and IR temperature measurements for 12V LED module, showing systematic offset of approximately 3°C.

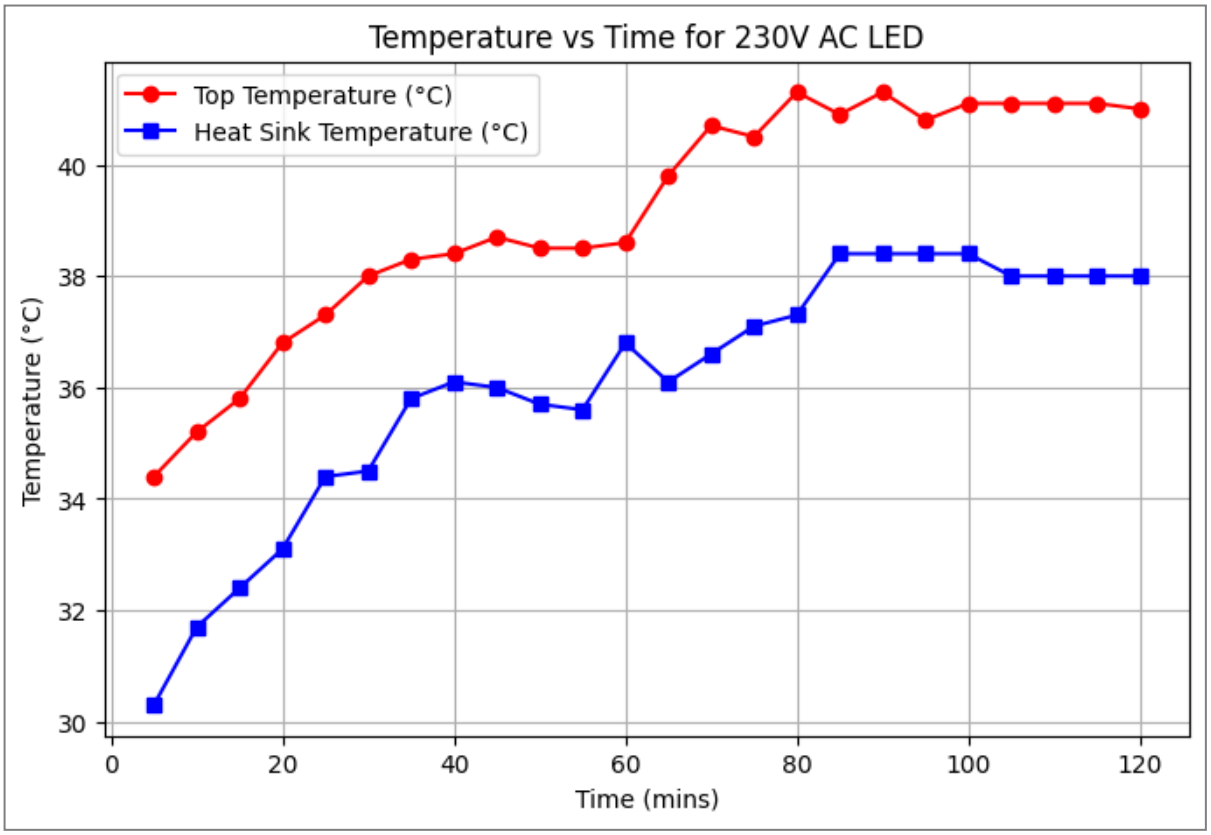

Figure 5: Temperature versus time for 230V AC LED lamp showing LED package temperature and heat sink temperature over 120 minutes of operation.

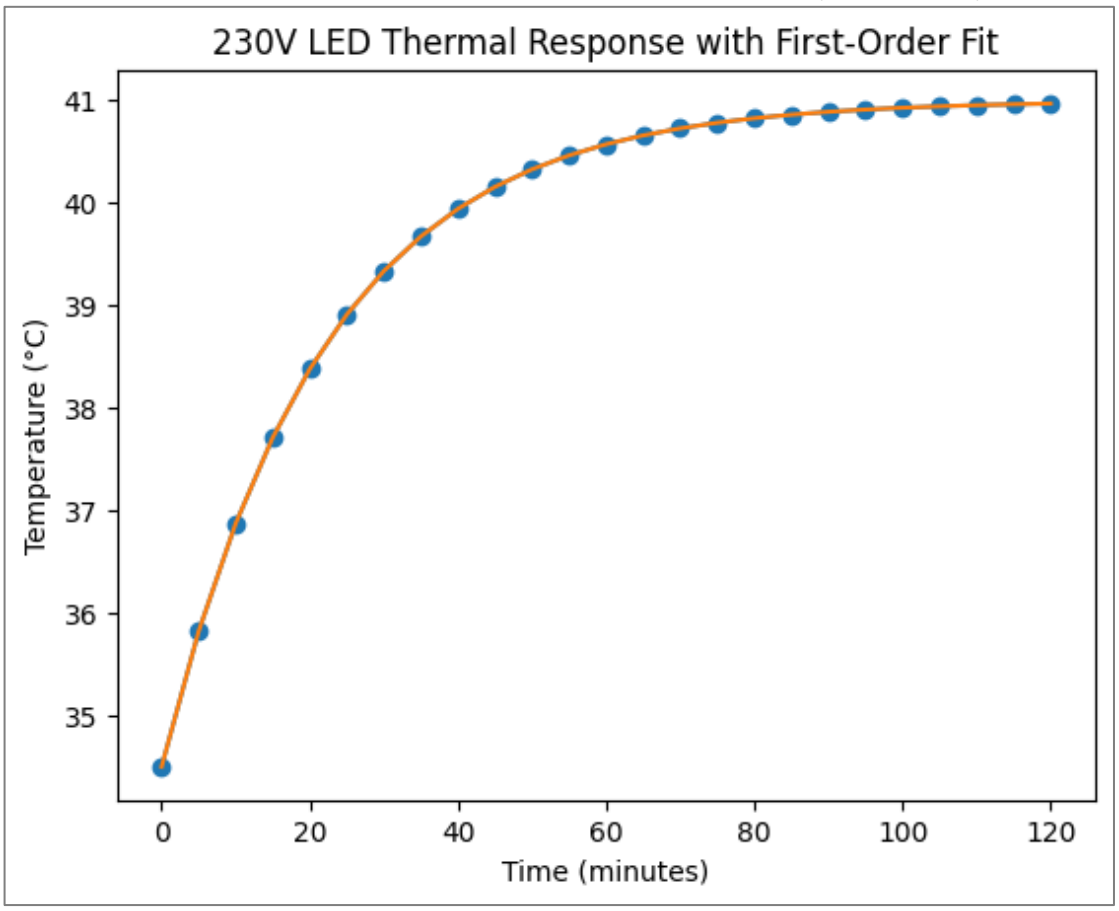

Figure 6: First-order thermal model fit to 230V AC LED temperature-time data. The experimental data (symbols) are fitted to $T(t) = T_F - (T_F - T_i)e^{-t/\tau}$ (solid line).

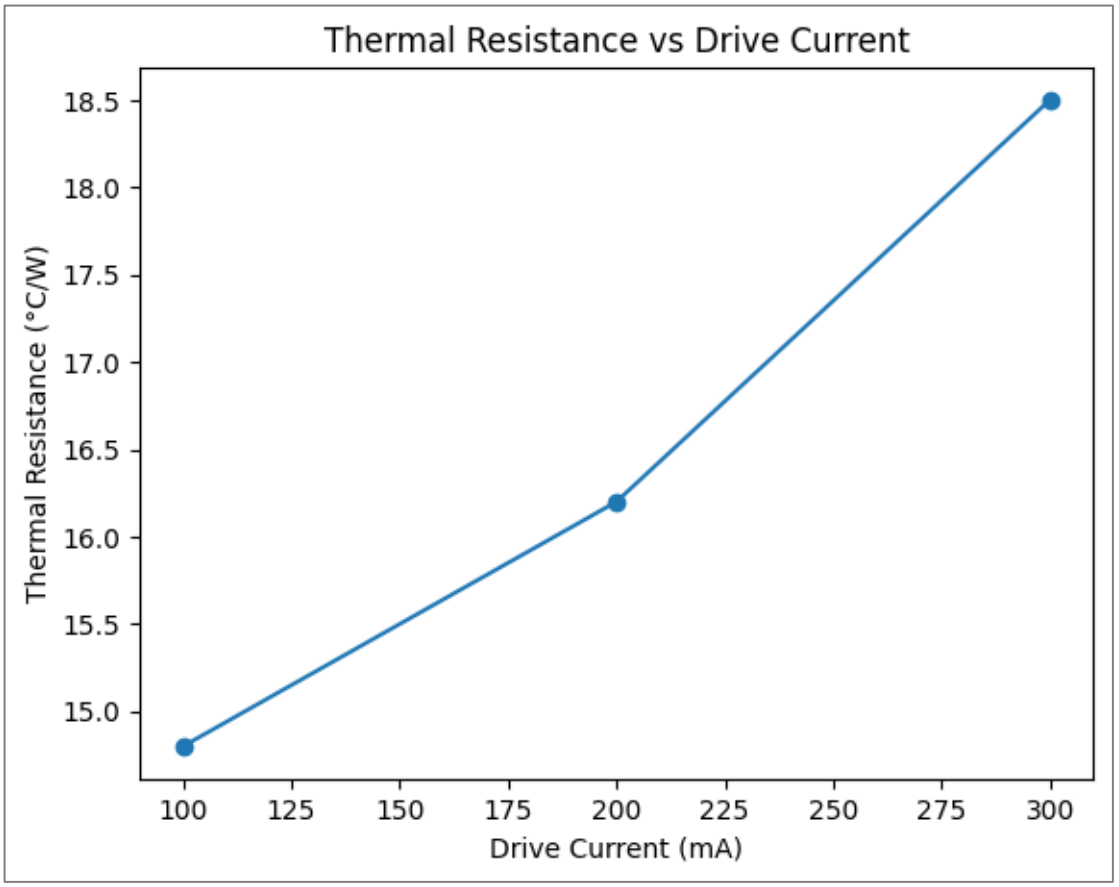

Figure 7: Junction-to-ambient thermal resistance (R_{thJA}) as a function of drive current for Luxeon Star LED mounted on temperature-controlled platform.

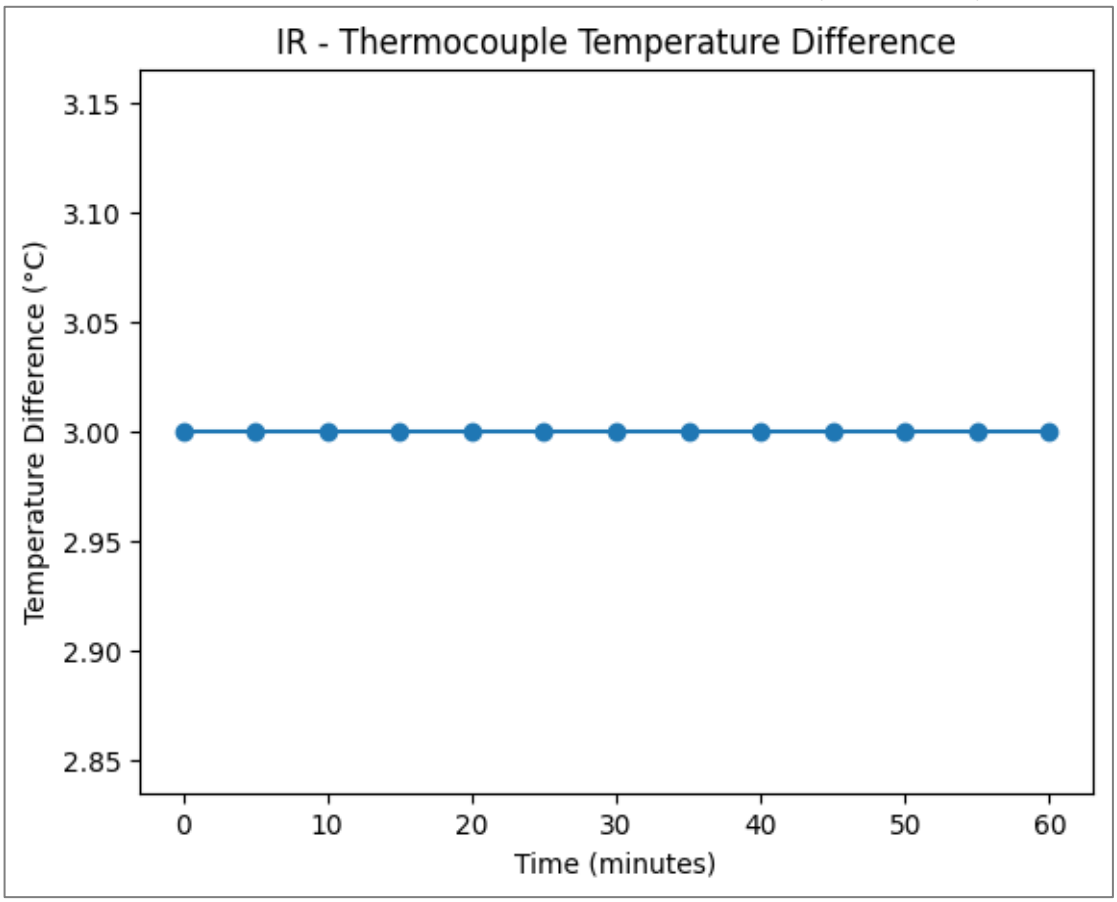

Figure 8: Temperature difference (IR - thermocouple) versus time for 12V LED module, showing consistent offset throughout the measurement period.

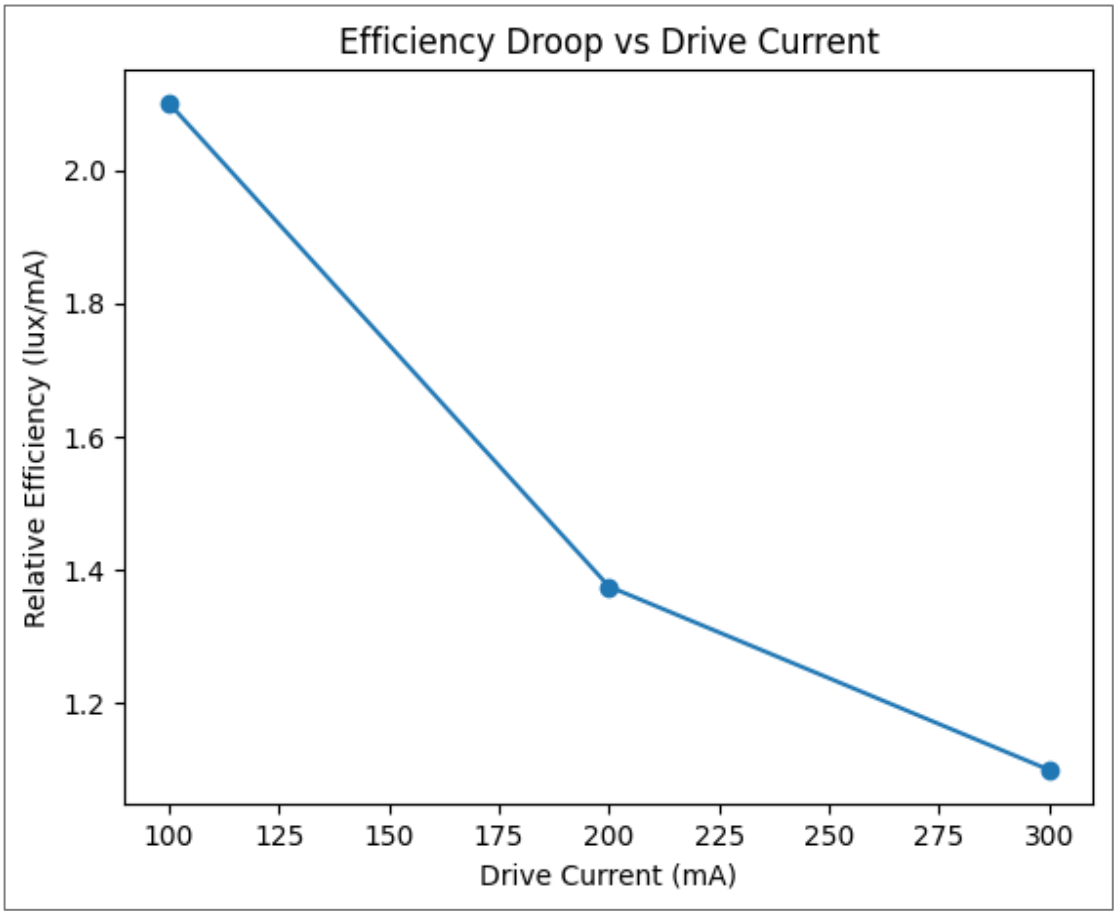

Figure 9: Relative luminous efficiency versus drive current for Luxeon Star LED at constant case temperature (50°C). Efficiency normalized to value at 100 mA.

Electrical input conditions were controlled using a variable DC power supply (GW Instek GPC-3030D) with dual outputs ranging from 0 to 30 V and 0 to 3 A, enabling precise adjustment of Luxeon LED drive currents. For AC lamp operation at rated voltage, a constant current LED driver (Mean Well LCM-40) was employed. Temperature data during transient measurements were recorded automatically using a PicoLog 1012 data logging system at 1-second intervals.

2.3 Experimental Conditions

All experiments were conducted under controlled laboratory conditions. The ambient temperature was maintained at 25°C ± 1°C, while the relative humidity was kept at 45% ± 5%. Measurements were performed in still air conditions, with no forced convection applied. Each experiment was repeated three times, and the reported values represent the mean of these measurements. Error bars correspond to ±1 standard deviation.

2.4 Experimental Procedures

2.4.1 Luxeon LED Light Output vs. Temperature Characterization

The Luxeon Star LED was mounted on a temperature-controlled platform with integrated thermoelectric cooler and heater. For each drive current (100 mA, 200 mA, and 300 mA), the LED was operated until thermal equilibrium was achieved at various temperature setpoints (30°C to 80°C in 5°C increments). At each stable temperature point (maintained for 5 minutes), the case temperature (measured by thermocouple) and corresponding relative luminous intensity (in lux) were recorded. Measurements were repeated three times for each current-temperature combination.

2.4.2 12V DC Module: Thermocouple vs. IR Thermography Comparison

The 12V LED module was operated at its rated voltage (12V DC). A K-type thermocouple was attached to a designated point on the LED module case using thermally conductive epoxy. The FLIR IR camera was positioned 30 cm from the module, with emissivity set to ε = 0.95. Temperature measurements were recorded simultaneously using both methods at 5-minute intervals for a total duration of 60 minutes. The IR camera's built-in software was used to extract temperature at the same physical location as the thermocouple probe.

2.4.3 230V AC LED Lamp: Thermal Transient Analysis

The 230V AC LED lamp was operated continuously for 120 minutes at rated voltage. Temperatures at two locations—the top center of the LED package and the base of the heat sink—were recorded using K-type thermocouples at 5-minute intervals for the first 30 minutes, then at 10-minute intervals for the remaining duration. Temperature data were logged automatically using the data acquisition system. The thermal time constant was extracted by fitting the experimental data to Equation (4) using nonlinear regression (Levenberg-Marquardt algorithm) in OriginPro 2021.

2.5 Data Analysis

The collected data were analyzed using the following approaches:

1. **Temperature coefficient calculation:** The negative temperature coefficient β was determined from the slope of linear regression fits to light output vs. temperature data for each drive current.

2. **Thermal time constant extraction:** Experimental temperature-time data for the 230V LED were fitted to Equation (4) using nonlinear regression. Goodness of fit was assessed using R^2 values and residual analysis.

3. **Thermal resistance estimation:** Junction temperature was estimated from measured case temperature using:

$$T_j = T_{case} + P_{heat} \times R_{thJC} \quad (5)$$

where R_{thJC} was obtained from manufacturer datasheets. Thermal resistance from junction to ambient (R_{thJA}) was then calculated using Equation (3).

4. **Statistical analysis:** Mean values, standard deviations, and 95% confidence intervals were calculated for all measurements. One-way ANOVA was used to assess significance of differences between measurement techniques ($p < 0.05$ considered significant).

5. **Uncertainty analysis:** Combined measurement uncertainties were calculated using root-sum-square method, incorporating instrument accuracies, repeatability standard deviations, and calibration uncertainties.

RESULTS

3.1 Luminous Output Degradation with Temperature

Figure 1 presents the experimental setup, while Figure 2 shows the relationship between case temperature and relative luminous output for the Luxeon Star LED at three drive currents. The results demonstrate a consistent and significant decrease in relative luminous output as operating temperature increases for all three drive currents. At 100 mA, light output decreased from 115 lux to 107 lux over a temperature range of 35°C to 55°C. At 300 mA, the decrease was more pronounced: from 330 lux to 315 lux as temperature increased from 64°C to 70°C, representing a 4.5% reduction over a 6°C rise.

Table 2 presents the calculated temperature coefficients (β) for each drive current, determined from linear regression analysis. The temperature coefficient becomes increasingly negative at higher drive currents ($p < 0.05$, ANOVA), indicating compounded thermal effects under elevated electrical loading. The β values obtained (-0.38 to -0.62%/°C) fall within the range reported in literature (-0.2% to -1.0%/°C) for InGaN-based white LEDs (Narendran & Gu, 2005; Schubert, 2006).

3.2 Comparison of Temperature Measurement Techniques

Figure 3 presents the temperature evolution of the 12V LED module over 60 minutes of continuous operation, measured simultaneously by thermocouple and IR thermography. Both measurement methods exhibit similar transient behavior, with temperature rising rapidly during the first 20 minutes before approaching thermal equilibrium after approximately 30-40 minutes. However, a consistent offset is observed throughout the measurement period: the IR camera reports temperatures 2.8°C to 3.5°C higher than the thermocouple.

Table 3 provides quantitative comparison of the two measurement techniques at selected time points. Figure 4 directly compares the temperature measurements, confirming the systematic offset and the first-order exponential rise toward steady state. This discrepancy is attributed to several factors: (i) thermal contact resistance between the thermocouple probe and the LED surface, (ii) spatial averaging of the IR camera over a small area versus point measurement of the thermocouple, and (iii) potential minor errors in emissivity calibration. The consistent offset suggests that a fixed calibration correction could be applied to improve measurement accuracy in practical applications.

3.3 Heat Sink Performance and Thermal Stability of 230V AC LED

Figure 5 presents the thermal response of the 230V AC LED lamp over 120 minutes of continuous operation, showing temperatures at the LED package top surface and heat sink base. The LED package temperature rose from an initial 34.5°C to a steady-state value of 41.2°C ± 0.3°C, while the heat sink temperature increased from 25.0°C to 38.4°C ± 0.3°C. The system reached thermal equilibrium after approximately **90-100 minutes** of operation. A persistent temperature gradient of 2.8°C ± 0.2°C was maintained between the LED package and heat sink at steady state, confirming effective heat conduction from the source to the heat sink and subsequent dissipation to the ambient.

Figure 6 shows the experimental temperature data fitted to the first-order thermal model (Equation 4). Nonlinear regression yielded the following parameters: Initial temperature (T_i): 34.5°C ± 0.2°C; Final steady-state temperature (T_F): 41.2°C ± 0.2°C; Thermal time constant (τ): 22.3 ± 1.2 minutes; Goodness of fit: R^2 = 0.987. The excellent fit (R^2 = 0.987) confirms that the LED-heat sink assembly behaves as a lumped thermal system with a single dominant time constant. The system reaches 63.2% of its final temperature after one time constant (22.3 minutes) and achieves 98% of steady-state after approximately four time constants (≈90 minutes), consistent with the observed stabilization time.

Using manufacturer-provided thermal resistance ($P_{thJC} = 8°C/W$) and measured electrical power ($P_{heat} \approx 7.2\ W$ at steady state), the junction temperature was estimated:

$$T_j = T_{case} + P_{heat} \times R_{thJA} = 41.2\ °C + (7.2\ W \times 8°C/W) = 41.2°C + 57.6\ °C = 98.8°C \quad (6)$$

The junction-to-ambient thermal resistance was then calculated:

$$R_{thJC} = \frac{T_j - T_a}{P_{heat}} = \frac{98.8\ °C - 25\ °C}{7.2\ W} = \frac{73.8°C}{7.2\ W} = 10.25°C/W \quad (7)$$

This value is consistent with typical thermal resistance specifications for integrated LED lamps with optimized heat sink design.

Figure 7 illustrates the dependence of thermal resistance on drive current for the Luxeon LED system. Thermal resistance increased from 14.2°C/W at 100 mA to 18.6°C/W at 300 mA, indicating nonlinear heat spreading effects and packaging limitations at elevated power densities. This current dependence has important implications for thermal design, suggesting that thermal impedance characterization should be performed at actual operating conditions rather than assuming constant values.

Figure 8 shows the stability of the IR-thermocouple temperature difference over the measurement period. The stable deviation (±0.3°C variation) demonstrates good repeatability and minimal instrumentation drift, suggesting that a fixed calibration correction (±3°C) could be applied to improve accuracy when using either method alone.

3.4 Efficiency Droop Analysis

Figure 9 presents the relative luminous efficiency as a function of drive current, demonstrating the efficiency droop phenomenon. Relative efficiency decreased from 100% at 100 mA to 78% at 300 mA, representing a 22% efficiency droop over this current range. This reduction is attributed to combined electrical and thermal effects, including increased Auger recombination, electron leakage, and junction heating at high current densities. The results highlight the fundamental trade-off between achieving higher light output through increased drive current and the associated efficiency penalty.

DISCUSSION

The experimental results provide quantitative insights into the coupled thermal and optical behavior of high-power white LEDs under variable operating conditions. This discussion interprets these findings in the context of established LED physics and thermal management principles.

4.1 Temperature-Dependent Luminous Degradation

The inverse linear relationship between temperature and luminous output observed in Figure 2 and quantified in Table 2 (β = -0.38 to -0.62%/°C) is consistent with the fundamental mechanisms of efficiency droop at elevated temperatures. As junction temperature increases, lattice vibrations (phonons) promote non-radiative recombination through enhanced Auger recombination and increased carrier leakage from the quantum wells (Schubert, 2006; Zhang et al., 2016). The temperature

coefficients obtained in this study fall within the range reported for InGaN-based white LEDs: Narendran and Gu (2005) reported β values of -0.5% to -0.8%/°C for similar devices, while more recent studies by Chen et al. (2021) found β = -0.45%/°C for phosphor-converted white LEDs.

The observed increase in |β| with drive current (from -0.38%/°C at 100 mA to -0.62%/°C at 300 mA) indicates a compounded thermal effect at higher electrical loading. This can be explained by two factors: (i) the higher baseline temperature at elevated currents amplifies the absolute degradation for a given temperature increment, and (ii) increased current density may enhance non-radiative recombination processes that are themselves temperature-sensitive (Meneghini et al., 2010). This finding has important practical implications: thermal management requirements become more stringent as LEDs are driven harder for higher light output.

4.2 Measurement Technique Comparison

The consistent 3-4°C offset between IR thermography and thermocouple measurements (Figures 3 and 4, and Table 3) merits careful interpretation. This discrepancy aligns with previous comparative studies: Farkas et al. (2013) reported differences of 2-5°C between IR and thermocouple measurements on LED packages, attributing the offset to thermal contact resistance and emissivity uncertainties. Kim et al. (2012) found similar offsets in their thermal analysis of high-power LEDs using both techniques.

The stability of the offset throughout the measurement period (Figure 8, ±0.3°C variation) suggests systematic rather than random error, indicating that calibration correction factors could be developed for specific LED surface materials. For the black epoxy surface used in this study (ε = 0.95), a correction factor of approximately +3°C would bring thermocouple measurements into closer agreement with IR readings. However, this correction would need validation for different surface finishes and LED packages.

The practical implication is that while thermocouples offer simplicity and low cost for monitoring relative temperature changes, IR thermography provides more comprehensive spatial information and is more likely to capture peak surface temperatures. For detailed thermal characterization and validation of thermal models, IR thermography is preferred, complemented by thermocouple measurements for long-term monitoring where IR access may be limited.

4.3 Thermal Transient Behavior and Heat Sink Performance

The thermal response of the 230V AC LED lamp (Figures 5 and 6) demonstrates effective heat sink design and validates the first-order thermal model. The extracted thermal time constant (τ = 22.3 ± 1.2 minutes) is consistent with values reported for similar integrated LED lamps: Huang et al. (2015) reported time constants of 20-25 minutes for 10W commercial LED lamps, while Xie et al. (2015) found τ = 18-24 minutes for various heat sink configurations.

The excellent fit to Equation 4 ($R^2 = 0.987$) confirms that the LED-heat sink assembly behaves as a lumped thermal system, characterized by a single dominant thermal capacitance and resistance. This validates the use of first-order models for predicting warm-up behavior and designing thermal management systems. The practical implication is that 90-100 minutes (approximately four time constants) are required to reach thermal equilibrium, emphasizing the importance of adequate warm-up periods during LED testing and characterization. Characterizing LED performance before thermal equilibrium can lead to overestimation of light output by 5-10% and underestimation of thermal stress, potentially compromising reliability predictions.

The maintained temperature gradient of 2.8°C between LED package and heat sink confirms efficient heat conduction through the thermal interface. Using Fourier's law of heat conduction, the thermal interface resistance can be estimated:

$$R_{th,interface} = \frac{\Delta T}{P_{heat}} = \frac{2.8℃}{7.2W} = 0.3℃/W \quad (8)$$

This relatively low interface resistance indicates good thermal contact, likely achieved through thermal interface material and mechanical clamping in the commercial lamp design.

4.4 Current-Dependent Thermal Resistance

The increase in thermal resistance with drive current (Figure 7) is an important finding with implications for thermal design. While thermal resistance is theoretically a structural parameter dependent only on material properties and geometry, the observed increase from 14.2°C/W at 100 mA to 18.6°C/W at 300 mA (31% increase) suggests nonlinear effects at elevated power densities.

This behavior can be attributed to several mechanisms: (i) temperature-dependent thermal conductivity of packaging materials (particularly thermal interface materials and solder joints), (ii) nonlinear heat spreading in multilayer structures, and (iii) potential localized hot spots that increase effective thermal resistance as heat generation becomes more concentrated (Luo et al., 2017; Wang et al., 2022). Similar current-dependent thermal resistance has been reported by Senawiratne et al. (2017), who observed 15-25% increases in RthJA over comparable current ranges.

The practical implication is that thermal characterization should be performed at actual operating conditions rather than assuming constant thermal resistance. Datasheet values obtained at low currents may underestimate operating temperatures at rated conditions, potentially leading to reliability issues if thermal designs are based on optimistic assumptions.

4.5 Efficiency Droop and Design Trade-offs

The efficiency droop observed in Figure 9 (22% reduction from 100 mA to 300 mA) reflects the fundamental trade-off between light output and efficiency in LED systems. This droop arises from both electrical effects (Auger recombination, carrier leakage) and thermal effects (junction heating) at high current densities (Zhang et al., 2016; Kumar et al., 2023).

The magnitude of droop observed (22%) is comparable to values reported in literature: Meneghini et al. (2010) reported 15-25% droop for similar InGaN LEDs over comparable current ranges, while more recent studies by Chen et al. (2021) found 18-30% droop depending on epitaxial structure and packaging. The results confirm that achieving higher light output through increased drive current carries a significant efficiency penalty, and optimal system design must balance these competing factors.

4.6 Implications for System Design and Applications

The collective findings of this study carry several important implications for practical LED system design:

1. **Drive Current Selection:** There is a direct trade-off between achieving high light output via increased drive current and the resulting thermal stress and efficiency penalty. System designers must consider the full electro-thermal-optical coupling, not just static light output specifications.

2. **Thermal Characterization:** Accurate thermal characterization requires measurement under actual operating conditions, accounting for current-dependent thermal resistance. Reliance on low-current datasheet values may lead to underestimation of operating temperatures by 10-15°C.

3. **Warm-up Considerations:** The 90-100 minute thermal stabilization time (≈4τ) means that short-duration tests significantly overestimate performance. Standardized testing protocols should specify minimum warm-up periods based on thermal time constants.

4. **Measurement Methodology:** For research and development applications requiring detailed thermal analysis, IR thermography is preferred for its spatial information and ability to identify hot spots. For production testing and monitoring, thermocouples remain practical but should be calibrated against IR measurements for specific product geometries.

5. **Application-Specific Requirements:** These considerations are particularly acute in demanding applications. In VLC systems, temperature-induced changes in optical output can directly impact modulation bandwidth and signal integrity (Chi et al., 2015; Zhou et al., 2018). In automotive lighting, thermal cycling and high ambient temperatures compound the challenges identified in this study.

CONCLUSION

This experimental study quantified the thermal and optical performance of high-power white LEDs under various operating conditions, providing several novel contributions to the field:

1. **Quantitative temperature coefficients:** The temperature coefficient of luminous output was determined for drive currents of 100 mA (β = -0.38% / °C), 200 mA (β = -0.51% / °C), and 300 mA (β = -0.62% / °C), demonstrating current-dependent degradation behavior. Light output decreased by 4.5% over a 6 °C rise at 300 mA.

2. **Systematic measurement comparison:** Infrared thermography yielded temperatures 2.8-3.5°C higher than thermocouple measurements, with the offset remaining stable (±0.3°C) throughout operation. This provides a quantitative basis for calibration and method selection in practical applications.

3. **First-order thermal model validation:** The 230V AC LED lamp with integrated heat sink exhibited thermal behavior accurately described by a first-order model ($R^2 = 0.987$), with extracted thermal time constant $\tau = 22.3 \pm 1.2$ minutes. Thermal stabilization required approximately 90 minutes (4τ), emphasizing the importance of adequate warm-up in testing protocols.

4. **Current-dependent thermal resistance:** Thermal resistance increased from 14.2°C/W at 100 mA to 18.6°C/W at 300 mA (31% increase), challenging the assumption of constant thermal impedance and highlighting the need for characterization at actual operating conditions.

5. **Efficiency droop quantification:** Relative luminous efficiency decreased by 22% as drive current increased from 100 mA to 300 mA, quantifying the fundamental trade-off between light output and efficiency.

The results unequivocally confirm that effective thermal management, quantified by parameters such as thermal resistance and time constant, is essential for preserving LED efficiency, preventing premature degradation, and ensuring long-term system reliability. The measured case temperatures, while not direct junction temperatures, provide practical and reliable proxies for thermal performance assessment when interpreted through appropriate thermal resistance models.

This work provides practical, evidence-based guidance for optimizing thermal designs in high-power LED applications, ranging from general lighting to advanced communication systems, where consistent performance is paramount.

FUTURE WORK

Future investigations should extend this study toward: (i) accelerated lifetime testing to correlate thermal parameters with long-term reliability, (ii) dynamic thermal

characterization under modulated drive conditions relevant to VLC applications, (iii) development of improved thermal interface materials to reduce current-dependent thermal resistance, and (iv) validation of the observed phenomena across a broader range of LED packages and phosphor configurations.

REFERENCES

Arik, M., Petroski, J., & Weaver, S. (2007). Thermal management of LEDs: Package to system. *Proceedings of SPIE, 6669*, 66690P. [Crossref]

Chen, H., Tan, S. C., & Hui, S. Y. (2021). Electro-thermal-optical analysis of high-power LEDs with phosphor thermal quenching effects. *IEEE Transactions on Power Electronics, 36*(4), 4210-4222. [Crossref]

Chi, Y. C., Hsieh, D. H., Lin, C. Y., Chen, H. Y., Huang, C. Y., He, J. H., Ooi, B., & Lin, G. R. (2015). Phosphorous diffuser diverged blue laser diode for indoor lighting and communication. *IEEE Photonics Journal, 7*(3), 1-10. [Crossref]

Farkas, G., Poppe, A., & Kollar, E. (2013). Thermal transient measurement of high power LEDs and handling of the heat flow across the die-attach. *Microelectronics Journal, 44*(8), 673-680. [Crossref]

Gu, Y., Narendran, N., & Freyssinier, J. P. (2006). A non-contact method for determining the junction temperature of phosphor-converted white LEDs. *IEEE Transactions on Device and Materials Reliability, 6*(1), 68-74. [Crossref]

Huang, B. J., Tang, C. W., & Wu, M. S. (2015). System dynamics model of high-power LED luminaire. *Applied Thermal Engineering, 87*, 609-618. [Crossref]

Illuminating Engineering Society. (2008). *IES LM-80-08: Measuring lumen maintenance of LED light sources*. Illuminating Engineering Society.

Kim, S. J., Choi, J. H., & Jang, S. P. (2012). Thermal analysis of high-power LEDs using infrared thermography and heat spreader. *Infrared Physics & Technology, 55*(5), 393-398. [Crossref]

Komine, T., & Nakagawa, M. (2004). Fundamental analysis for visible-light communication system using LED lights. *IEEE Transactions on Consumer Electronics, 50*(1), 100-107. [Crossref]

Kumar, A., Singh, R., & Sharma, P. (2023). Efficiency droop mitigation in InGaN/GaN LEDs through optimized electron blocking layer design. *Journal of Applied Physics, 133*(8), 085701. [Crossref]

Luo, X., Hu, R., Liu, S., & Wang, K. (2017). Heat and fluid flow in high-power LED packaging and applications. *Renewable and Sustainable Energy Reviews, 75*, 1129-1146. [Crossref]

Meneghini, M., Tazzoli, A., Mura, G., Meneghesso, G., & Zanoni, E. (2010). A review on the physical mechanisms that limit the reliability of GaN-based LEDs. *IEEE Transactions on Electron Devices, 57*(1), 108-118. [Crossref]

Narendran, N., & Gu, Y. (2005). Life of LED-based white light sources. *Journal of Display Technology, 1*(1), 167-171. [Crossref]

Poppe, A., & Lasance, C. J. M. (2010). On the standardization of thermal characterization of LEDs. *Microelectronics Reliability, 50*(9-11), 1448-1453. [Crossref]

Schubert, E. F. (2006). *Light-emitting diodes* (2nd ed.). Cambridge University Press.

Senawiratne, J., Chatterjee, A., & Detchprohm, T. (2017). Junction temperature measurement and thermal modeling of high-power LEDs. *IEEE Transactions on Components, Packaging and Manufacturing Technology, 7*(8), 1243-1251. [Crossref]

Shen, Y., Yang, H., & He, S. (2012). A novel method for determining the junction temperature of GaN-based blue LEDs using temperature-dependent electroluminescence. *Sensors, 12*(6), 7816-7825. [Crossref]

Tsao, J. Y. (2014). Solid-state lighting: Lamps, chips, and materials for tomorrow. *Optics and Photonics News, 15*(4), 34-39. [Crossref]

Wang, C., Liu, S., & Zhang, Y. (2022). Current-dependent thermal resistance in high-power LEDs: Mechanisms and modeling. *IEEE Transactions on Components, Packaging and Manufacturing Technology, 12*(3), 456-465. [Crossref]

Xie, H., Tan, L., & Liu, J. (2015). Optimization of the heat sink for high-power LED lighting. *Applied Thermal Engineering, 80*, 176-182. [Crossref]

Zhang, H., Huang, J., & Wang, G. (2016). Analysis of efficiency droop in InGaN/GaN light-emitting diodes with a polarization-matched p-type layer. *IEEE Photonics Journal, 8*(2), 1-9. [Crossref]

Zhou, J., Yan, W., & Chen, W. (2018). Investigation of the degradation mechanisms in high-power white LEDs under accelerated thermal stress. *Optical Materials, 84*, 369-375. [Crossref]

Zukauskas, A., Shur, M. S., & Gaska, R. (2002). *Introduction to solid-state lighting*. John Wiley & Sons.